

# Robust inference of causality in high-dimensional dynamical processes from the Information Imbalance of distance ranks

Vittorio Del Tatto<sup>1</sup>, Gianfranco Fortunato<sup>1</sup>, Domenica Bueti<sup>1</sup>, and Alessandro Laio<sup>1,2</sup>

<sup>1</sup>Scuola Internazionale Superiore di Studi Avanzati, SISSA, via Bonomea 265, 34136 Trieste, Italy

<sup>2</sup>ICTP, Strada Costiera 11, 34151 Trieste, Italy

## Abstract

We introduce an approach which allows inferring causal relationships between variables for which the time evolution is available. Our method builds on the ideas of Granger Causality and Transfer Entropy, but overcomes most of their limitations. Specifically, our approach tests whether the predictability of a putative driven system  $Y$  can be improved by incorporating information from a potential driver system  $X$ , without making assumptions on the underlying dynamics and without the need to compute probability densities of the dynamic variables. Causality is assessed by a rigorous variational scheme based on the Information Imbalance of distance ranks, a recently developed statistical test capable of inferring the relative information content of different distance measures. This framework makes causality detection possible even for high-dimensional systems where only few of the variables are known or measured. Benchmark tests on coupled dynamical systems demonstrate that our approach outperforms other model-free causality detection methods, successfully handling both unidirectional and bidirectional couplings, and it is capable of detecting the arrow of time when present. We also show that the method can be used to robustly detect causality in electroencephalography data in humans.

## Introduction

The aim of discovering causal relationships among observable quantities has been inspiring and guiding scientific research from its dawn, as causality is at the very heart of physical phenomena and natural laws. While dealing with experimental data, correlation measures are frequently associated with causality, even though correlation alone is neither a necessary nor a sufficient condition for causation [1]. Determining causality from data collected without directly intervening on the system under study - namely, without performing interventional experiments where the causal variable is manipulated - is a challenging problem which received increasing attention over the last decades [2, 3]. The variety of statistical tools used to achieve this goal largely grounds on the pioneering works of Steve Granger in time-series analysis [4] and Judea Pearl in causal inference on networks [5]. The application of such tools to observational data is particularly crucial when experiments are unfeasible or unethical, such as in the case of medical studies that would create a real risk for patient's health, or Earth science researches that could alter delicate ecological balances, just to give a few examples.

When data are recorded in the form of time series, causality can in principle be detected without experimental intervention. Several approaches have been developed for this purpose, leading to significant breakthroughs in diverse fields, from economics [4, 6] to ecology [7] to Earth system sciences [8] and neuroscience [9–11]. The key idea at the basis of these approaches is detecting the presence of asymmetric couplings between the dynamic variables. However,

some important conceptual and practical problems remain open and are still object of intense investigation [12–14]. One problem stems from the memory that the caused (or driven) variables carry about the causal (or driver) ones, which acts as an internal confounding mechanism that may lead to false coupling detections. For example, the fact that a system  $X$  drives a system  $Y$  may result into a dependence between the present state of  $Y$  and the future state of  $X$ . Such dependence has no causal origin, but could be misinterpreted as a dynamical coupling in direction  $Y \rightarrow X$ . Additionally, the fact that real-world time series often emerge from complex underlying dynamics naturally brings to the necessity of methodologies dealing with high-dimensional data [13], facing the so-called curse of dimensionality.

From a historical perspective, the first quantitative criterion to measure causality dates back to the work of Wiener [15], who observed that the prediction of a signal  $Y$  can be improved by using the past information of a signal  $X$  if  $X$  is causal to  $Y$ . Inspired by Wiener, Granger proposed to identify causal links in time series analysis with a vector autoregressive model assuming a linear dynamics [4]. Since then, several nonlinear generalizations of Granger's idea have been proposed [16–21].

Two measures for causality detection that are implicitly based on a similar predictability principle are Transfer Entropy [22] and Conditional Mutual Information [23]. These methods, which were proposed independently but shown to be equivalent [24], rely on information-theoretic quantities aiming to detect asymmetries in the couplings between time-dependent systems. Transfer Entropy has been proven to be

equivalent to Granger causality for Gaussian variables [25], which means that both the methods can be naturally interpreted as its information-theoretic generalization. However, computing *multivariate* probability distributions for mutual informations and relative entropies can be challenging and suffers from the curse of dimensionality, requiring to work with conditional probabilities of a few variables at a time [26]. For this reason, alternative methods that do not require to compute or approximate the probability distributions of the dynamic variables are more appealing for real-world applications.

Among these, cross mapping methods rely on Takens' theorem [27], which allows to reconstruct a dynamical system's attractor - or rather a version capturing its main features, called *shadow manifold* - using one-dimensional time series. This reconstruction is carried out by mapping each point in a vector, named time-delay embedding, which includes points in its recent past. In particular, Convergent Cross Mapping [7] evaluates the coupling strength  $X \rightarrow Y$  by attempting a local reconstruction of the shadow manifold of  $X$  from the shadow manifold of  $Y$  and computing a correlation coefficient between the reconstructed and the ground-truth points. The reconstruction attempt is repeated over different lengths of the time series, since the correlation is expected to converge as a function of the number of data points when the coupling is present. A more recent cross mapping method, known as measure  $L$  [28], employs a similar approach but carries out the local reconstruction of the target manifold using ranks rather than distances. As representatives of the Granger causality framework we mention the Extended Granger Causality test [16] and the Predictability Improvement method [20]. The former confines the linear approximation of the dynamics to local regions in the state space and averages the results over the entire state portrait, while the latter carries out predictions in the spaces of time-delay embeddings using a variant of the method of analogues [29].

In this study we introduce a causality detection method falling within the framework of Granger causality and partially related both to the measure  $L$  and to the Predictability Improvement approach, but overcoming some important drawbacks of these methods. Our approach is based on Information Imbalance [30], a statistical measure designed to compare distance spaces. By measuring distances between independent realizations of the same dynamical process, the method evaluates whether including the putative driver variables in the distance space built at time  $t$  allows to better guess which pairs of trajectories are closest in the space of the driven variables at a future time  $t + \tau$ . The intuition behind this approach is that close realizations of a process are expected to remain close along their time evolution if the distance between them is measured by using all the relevant dynamic variables. The approach's robustness and

effectiveness stem from analyzing the statistics of distance ranks and examining how it is affected by the inclusion of potential causal variables in the distance definition. As a consequence, the method does not suffer from the limitations of measures such as Transfer Entropy / Conditional Mutual Information in high-dimensional systems. The information of the driver system is added to the space built in the past using a variational approach, which allows probing the presence or absence of a coupling within a theoretically rigorous framework. To assess the validity of the method we carried out tests on a variety of coupled dynamical systems with both unidirectional and bidirectional couplings, as well as on real-world time series from electroencephalography (EEG) experiments. These tests led us to observe that our method

- allows recognizing unambiguously when a causal coupling is *absent*, at variance with all the other approaches we tested;
- provides reliable and robust results also when the dynamics system is *high-dimensional*, such as the electrophysiological signal of a human brain, or a Lorenz 96 system;
- can be used together with state space reconstruction techniques when not all the dynamic variables are observed;
- allows detecting the *arrow of time* in causality, even in high-dimensional systems, overcoming the aforementioned problem of false positives induced by time-correlation and memory effects.

## The Information Imbalance Gain

The Information Imbalance is a statistical measure introduced to compare the information content of two distances  $d_A$  and  $d_B$  defined on a set of points, which allows assessing whether they are equivalent, independent or if one is more informative than the other, in terms of their ability to accurately describe the underlying data [30]. The relative information content of two distance spaces can be measured, in principle, by the conditional entropy of one distance, given the other. Like all differential entropies, however, this quantity is not invariant with respect to invertible maps such as simple scalings  $d' = ad$  [31], even if the two distances  $d$  and  $d'$  related by such transformations are equivalent. To solve this problem, in Ref. [30] we proposed to perform a *copula transformation* on the distance distributions and to use the conditional entropy  $H(c_B | c_A < \varepsilon)$  in the limit  $\varepsilon \rightarrow 0$ , where  $c_A$  and  $c_B$  are the copula variables of the pair-wise distances in  $d_A$  and  $d_B$ . Since a copula transformation is always invertible, the inequality  $c_A < \varepsilon$  can be translated into a constraint over small distances in space  $A$ .

This constraint is invariant with respect to invertible distance transformations.

In practical applications, a useful proxy of the conditional entropy  $H(c_B | c_A < \varepsilon)$ <sup>1</sup> is provided by a simple average over the ranks that we called Information Imbalance. The Information Imbalance from distance  $A$  to distance  $B$  is the average rank according to distance  $d_B$  restricted to points which are close according to  $d_A$ :

$$\Delta(A \rightarrow B; k) = \frac{1}{k} \sum_{h=1}^k \frac{2}{N} \langle r^B | r^A = h \rangle = \frac{2}{N} \langle r^B | r^A \leq k \rangle, \quad (1)$$

where  $N$  is the number of points and  $r_{ij}^A$  (resp.  $r_{ij}^B$ ) is the distance rank of point  $j$  with respect to point  $i$  according to distance  $A$  (resp.  $B$ ). The parameter  $k$  specifies the number of neighbors taken into account and generalizes the definition in Ref. [30], which assumes  $k = 1$ . A larger  $k$  decreases the statistical error associated to the Information Imbalance but, at the same time, increases its bias as a proxy of the conditional entropy  $H(c_B | c_A < \varepsilon)$ . The prefactor  $2/N$  statistically confines this quantity between 0 and 1, which are the limits of  $d_A$  being respectively maximally and minimally informative with respect to  $d_B$ . As further discussed in the SI, in this form Information Imbalance is equivalent to the measure  $L$  introduced by Chicharro and Andrzejak in [28] for studying coupled dynamical systems.

In Ref. [30], it was shown empirically that Information Imbalance makes it possible to recover the arrow of time

<sup>1</sup>actually of its derivative with respect to  $\varepsilon$ , see SI.

from time series data. Here we propose to use a generalization of this approach to evaluate the presence of causal relationships among sets of time-dependent variables, using no prior knowledge about the underlying dynamics. To set the framework, let  $X(t)$  and  $Y(t)$  be vectors characterizing the states of two dynamical systems at time  $t$ , with components  $x_\alpha(t)$  and  $y_\beta(t)$  ( $\alpha = 1, \dots, D$ ;  $\beta = 1, \dots, D'$ ). Since the Information Imbalance is computed over a set of points, we suppose to have access to multiple experiments  $X^i(t)$  and  $Y^i(t)$  ( $i = 1, \dots, N$ ), representing independent realizations of identical copies of the systems. Our causality detection method relies on the intuition that if a dynamic variable  $X$  causes another variable  $Y$  and one attempts to make a prediction on the future of  $Y$ , a distance measure built using the present states of both  $X$  and  $Y$  will have more predictive power than a distance built using only  $Y$ . This idea is depicted in Fig. 1. Formally, we postulate that if  $X$  causes  $Y$ , there exists at least a value of  $\alpha > 0$  such that

$$\Delta(\alpha) := \Delta((\alpha X(t), Y(t)) \rightarrow Y(t + \tau)) < \Delta(Y(t) \rightarrow Y(t + \tau)). \quad (2)$$

Here  $\alpha$  plays the role of a scaling parameter for the units of  $X$  accounting at the same time for the magnitude of the coupling strength and for intrinsic differences between the two systems.  $\tau$  is a positive parameter representing the time lag of the information transfer from the driving to the driven system. Since this parameter only appears in the argument of the putative driven system  $Y$ , the approach is still valid

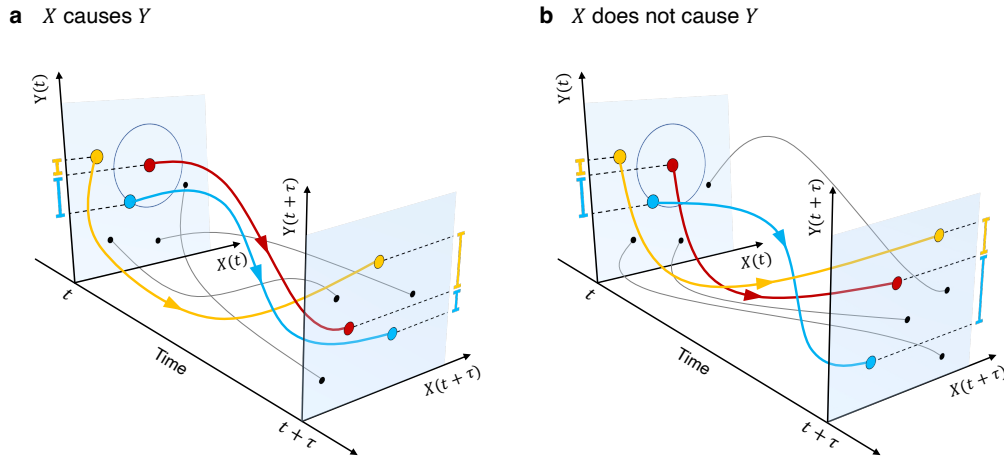


**Figure 1.** Illustration of the method applied to the  $X \rightarrow Y$  direction. Different lines represent independent realizations of the same dynamical process in the space  $(X, Y)$ . Both in **a** and in **b** the reference trajectory is depicted in red. At time  $t$  the blue trajectory is the closest in space  $(X(t), Y(t))$ , while the yellow realization is the closest in the marginal space  $Y(t)$ . When we look at distances in the marginal space  $Y(t + \tau)$ , **a**) if  $X$  causes  $Y$  it is likely that the closest curve is the blue one, which was the closest in the full dynamical space, while **b**) if  $X$  does not cause  $Y$  the yellow trajectory remains the closest, as the space  $Y(t)$  already contains the maximal information to predict the state of  $Y$  at time  $t + \tau$ .

when  $Y$  is a dynamical system and  $X$  is a static variable, with the caveat that in this scenario causality can only be tested in direction  $X \rightarrow Y$ . Using Eq. (2) we can recast the problem of causality detection into a variational optimization task, where the goal is to find the minimum of  $\Delta(\alpha)$ . With this goal, we define the Imbalance Gain as the relative difference between the Information Imbalance on the right-hand side of Eq. (2), corresponding to the case  $\alpha = 0$ , and the one on the left-hand side, minimized with respect to  $\alpha$ :

$$\delta\Delta := \frac{\Delta(\alpha = 0) - \min_{\alpha} \Delta(\alpha)}{\Delta(\alpha = 0)}. \quad (3)$$

We highlight that the Imbalance Gain is by construction a positive definite quantity. According to our definitions, the coupling  $X \rightarrow Y$  is present if  $\delta\Delta > 0$  and it is absent when  $\delta\Delta = 0$ , i.e. when the minimum of  $\Delta(\alpha)$  is found for  $\alpha = 0$ . In the first scenario, we use the value of the Imbalance Gain in order to compare the strengths of different causal couplings.

This approach can be naturally interpreted as a generalization of Granger causality, as it examines the impact of introducing the supposed causal variable in the past on the predictability of the supposed caused variable in the future. However, due to the variational formulation which is implicit in Eq. (3), our approach allows recognizing rigorously whether a dynamic variable does not cause another variable: in this situation,  $\delta\Delta = 0$ . Similarly to Transfer Entropy based approaches [22, 23], the choice of the time lag  $\tau$  plays an important role as it modulates the magnitude and detectability of the causal effects: for small values of  $\tau$  the signal is expected to be weak even when the interaction is instantaneous, for processes which are continuous. Instead, in the limit of large  $\tau$  it shrinks to zero, as the state of the system becomes unpredictable from the knowledge of the initial conditions.

Ideally, the distance spaces appearing in Eq. (2) should be constructed using all the components  $x_{\alpha}(t)$  and  $y_{\beta}(t)$ . However, in real experiments it is common that not all the variables of each system are recorded. In this case, Takens' theorem [27] ensures that it is possible to recover the information of the missing coordinates by means of the time-delay embeddings of the known variables. For example, if only coordinate  $x_1(t)$  is recorded for system  $X$ , one can construct the vectors  $\tilde{x}_1(t) = (x_1(t), x_1(t - \tau_e), x_1(t - 2\tau_e), \dots, x_1(t - (E - 1)\tau_e))$  and the projection of the trajectory in this space is guaranteed to be topologically equivalent to the original orbit for almost any choice of the embedding time  $\tau_e$ , provided that the embedding dimension  $E$  is at least twice larger than the dimension of the original attractor. In practice,  $\tau_e$  is typically set as the first minimum of the lagged mutual information  $I(x_1(t), x_1(t + \tau))$  [32] in order to construct

the delay embeddings with samples as independent as possible, while  $E$  is determined with the false nearest neighbor approach [33]. However, the optimal values of these parameters generally depend on the specific prediction or phase-space reconstruction method employing them [34].

In the following Section we show the application of our method to several dynamical systems displaying a chaotic behaviour, namely a high sensitivity to the initial conditions, and to real-world EEG time series. Throughout the tests we only employed two values of the parameter  $k$ :  $k = 1$  - which gives the most unbiased estimate of the Imbalance Gain - for low-dimensional system, and  $k = 20$  - which decreases the statistical error associated to our causality measure - for high-dimensional ones.

## Results

In order to benchmark our procedure, we first studied the qualitative behaviour of the Information Imbalance  $\Delta(\alpha)$  in the optimal scenario where all the coordinates of each system are known, so that the use of time-delay embeddings is unnecessary. We employed Rössler systems (see Methods - Dynamical systems) and considered three different coupling configurations, where the link is unidirectional between identical systems (Fig. 2a), unidirectional between different systems (Fig. 2b) and bidirectional between identical systems (Fig. 2c). In these preliminary tests the number of neighbors  $k$  was set to 1 and the time lag  $\tau$  was fixed to 5. In the case of unidirectional coupling (Fig. 2, panels a and b),  $\Delta(\alpha)$  monotonically increases in the direction where the causal link is absent ( $Y \rightarrow X$ ), while it clearly shows the presence of a minimum in the correct coupling direction ( $X \rightarrow Y$ ). Qualitatively the presence of this minimum indicates that adding the information on the value of  $X$  helps predicting the future of  $Y$ . The absence of a minimum in the reverse directions indicates instead that adding the information on the value of  $Y$  can only degrade the predictability of the future of  $X$ . Consistently with this scenario, if the coupling is bidirectional the Information Imbalance shows clear minima as a function of  $\alpha$  in both directions (Fig. 2c).

To demonstrate the robustness of the procedure more quantitatively, in Fig. 3 we report a comparison of our method with three alternative approaches for causality detection, namely the Extended Granger Causality [16], Convergent Cross Mapping [7] and the Measure  $L$  [28]. The latter two approaches are nonparametric, like ours, while the former is based on an autoregressive model. As the other methods employ time-delay embeddings, to ensure a fair comparison we also employed the delayed representations of single coordinates ( $x_1$  and  $y_1$ ). Fig. S3 in the SI reports the results of our method using all the coordinates of each system. The metaparameters of each approach were opti-

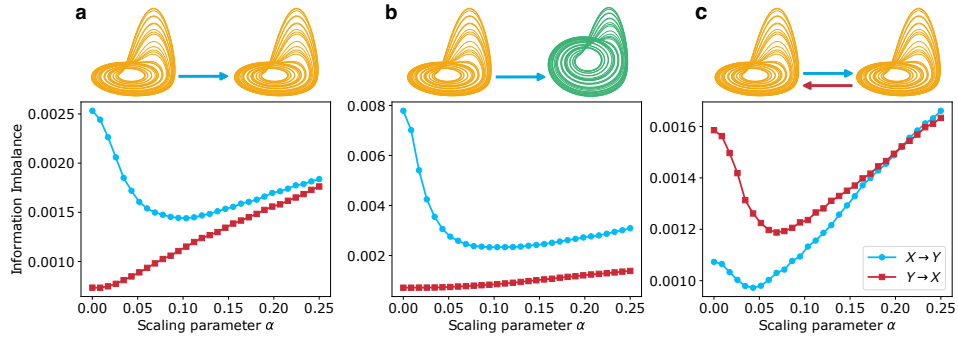


**Figure 2.** Profiles of the Information Imbalance  $\Delta(\alpha)$  as a function of  $\alpha$ , to assess the presence of the  $Y \rightarrow X$  and  $X \rightarrow Y$  causal links. The three panels refer to different pairs of Rössler systems: **a)** identical and unidirectionally coupled with coupling strength  $\varepsilon = 0.1293$ , **b)** different and unidirectionally coupled with  $\varepsilon = 0.1293$ , **c)** identical and bidirectionally coupled with  $\varepsilon_{X \rightarrow Y} = 0.0603$  and  $\varepsilon_{Y \rightarrow X} = 0.1$ .

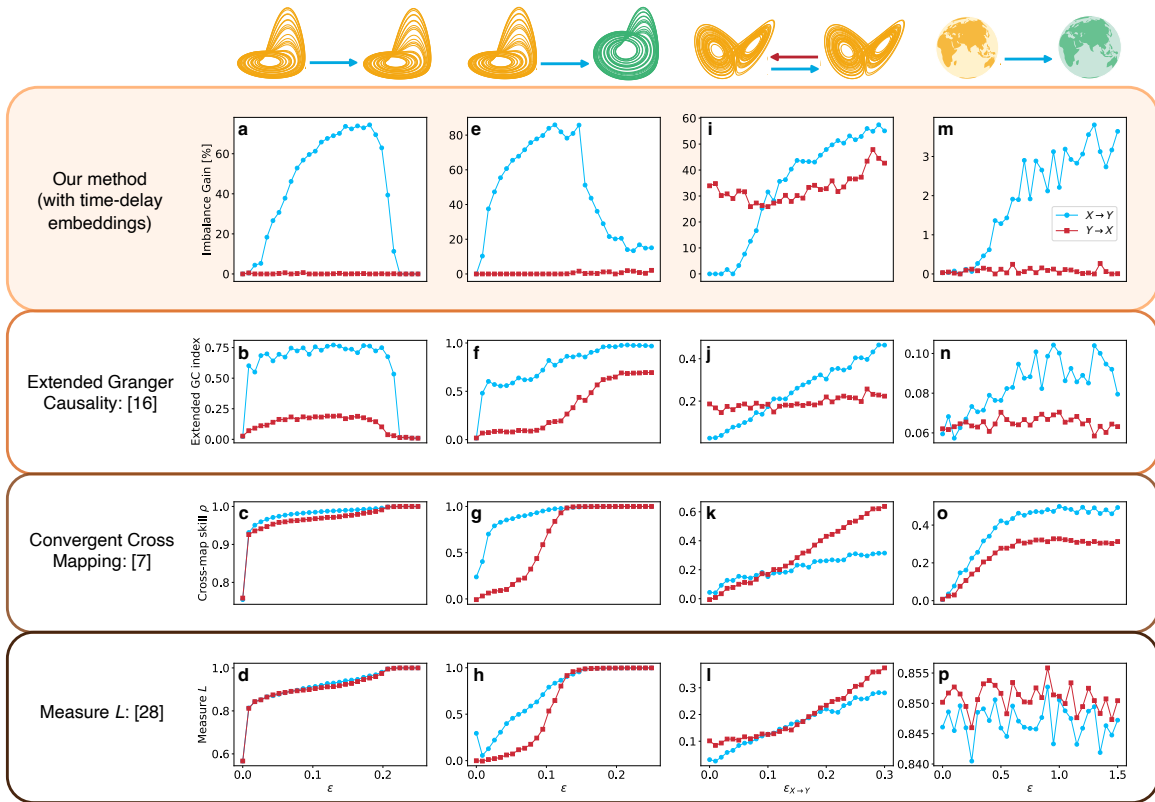


**Figure 3.** Comparison of different causality detection methods applied to four pairs of coupled dynamical systems. The results are shown as a function of the coupling parameter  $\varepsilon$  (or  $\varepsilon_{X \rightarrow Y}$  in the bidirectional case). **a-d)**: Identical and unidirectionally coupled Rössler systems. **e-h)**: Different and unidirectionally coupled Rössler systems. **i-l)**: Unidirectionally coupled Lorenz systems. The independent variable is the parameter for the  $X \rightarrow Y$  link; the opposite coupling  $\varepsilon_{Y \rightarrow X}$  was fixed to 0.1. **m-p)**: Unidirectionally coupled Lorenz 96 systems, with 40 variables each. The parameters employed to compute the Imbalance Gain are **a-b)**  $\tau = 20$ ,  $k = 1$ ,  $E = 3$ ,  $\tau_e = 1$ , **c)**  $\tau = 5$ ,  $k = 1$ ,  $E = 3$ ,  $\tau_e = 1$  and **d)**  $\tau = 30$ ,  $k = 20$ ,  $E = 30$ ,  $\tau_e = 1$ .

mized independently, as reported in the Methods section. The set of tests was carried out using four different pairs of dynamical systems: two low-dimensional and unidirectionally coupled (identical and different Rössler systems, Figs. 3a-d and Figs. 3e-h), one low-dimensional and bidirectionally coupled (Lorenz systems, Figs. 3i-l) and one high-dimensional and unidirectionally coupled (Lorenz 96 systems, Figs. 3m-p). In the low-dimensional and unidirectional coupling scenario (Figs. 3a-h) our method successfully finds a unidirectional link  $X \rightarrow Y$ , displaying absent or negligible causality in the  $Y \rightarrow X$  direction. The sharp decays observed in Fig. 3a and Fig. 3e occur in correspondence of the *synchronization transitions* of the two systems, namely when the trajectories of  $X$  and  $Y$  become biunivocally related. In this regime, it has been argued that it is not possible to detect the correct coupling direction anymore [35]. The other approaches correctly detect that causality is stronger in the  $X \rightarrow Y$  direction than in the reverse direction. However, in all the other approaches it is not possible to deduce from the data that the coupling in the  $Y \rightarrow X$  direction is absent. This is a major improvement of our approach. In the bidirectional case (Figs. 3i-o) all the methods correctly detect the presence of both the causal links, but only the Imbalance Gain and the extended GC index predict the correct ranking of the two coupling strengths for  $\varepsilon_{X \rightarrow Y} \gtrsim 0.1$ . Consistently, in both the methods the curves quantifying the strengths of the two causal links intersect at  $\varepsilon_{X \rightarrow Y} \simeq 0.1$ , which is the value at which the opposite coupling parameter  $\varepsilon_{Y \rightarrow X}$  was fixed.

In the high-dimensional scenario (Figs. 3m-p) our mea-

sure displays the highest relative difference between the signals in the two directions, and the Imbalance Gain in the  $Y \rightarrow X$  direction is almost zero, with only small fluctuations which can be ascribed to statistical errors. The Extended Granger Causality and the Convergent Cross Mapping approaches detect the correct order of the causal coupling but, once again, do not allow concluding that causality is actually absent in one direction. Finally, the Measure L approach provides for this system the wrong order in the causality coupling.

**The arrow of time from the Imbalance Gain.** To test the sensitivity of our method to different choices of the delay time  $\tau$  between the “present” and the “past”, we computed the Imbalance Gain as a function of this parameter for two Rössler systems and two Lorenz 96 systems, both with unidirectional link  $X \rightarrow Y$  (Fig. 4). When the coupling is time-independent, as in all the examples considered so far (Figs. 4a-b), we notice that our measure brings to similar Imbalance Gain curves both for positive and negative values of  $\tau$ . This is qualitatively consistent with what observed in Ref. [36], where it was argued that coupled dynamic systems apparently violate the first Granger causality principle of the effect following the cause. However, the Imbalance Gain  $X \rightarrow Y$  is stronger when  $\tau$  is positive, namely in the future. Therefore, at odds with what reported in Ref. [36], the quantitative comparison of the magnitudes of the Imbalance Gain for positive and negative time lags allows to clearly detect the arrow of time of the series.

Here we stress the fact that these systems feature very

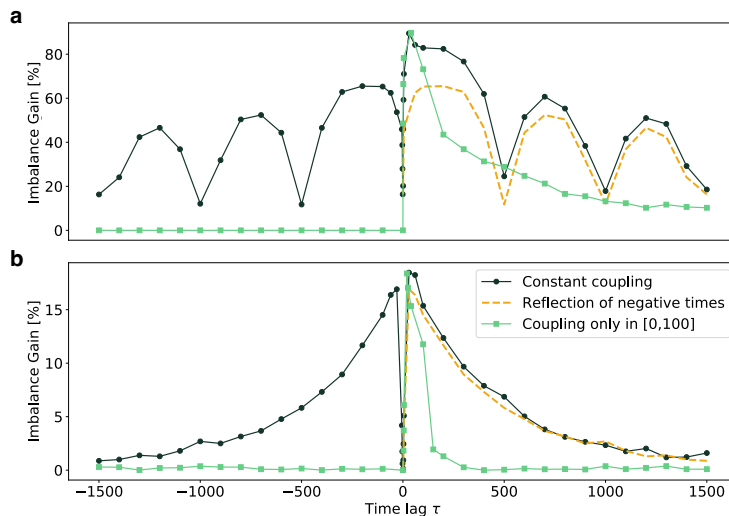


**Figure 4.** Behaviour of the Imbalance Gain in the  $X \rightarrow Y$  direction as a function of the parameter  $\tau$ . **a)** unidirectionally coupled and different Rössler systems with  $\varepsilon = 0.1035$ , using  $k = 1$ . **b)** unidirectionally coupled Lorenz 96 systems with  $F_X = 5$ ,  $F_Y = 6$  and  $\varepsilon = 1$ , using  $k = 20$ .

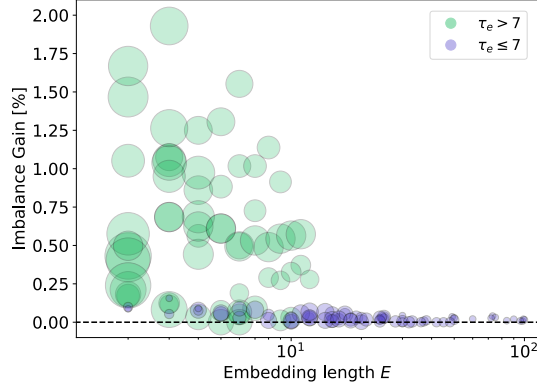


**Figure 5.** Imbalance Gain as a function of the embedding length  $E$ , computed in direction  $Y \rightarrow X$  for two Lorenz 96 systems with opposite link  $X \rightarrow Y$  ( $F_X = 6$ ,  $F_Y = 4$ ,  $\varepsilon = 1$ ), using  $k = 20$  and  $\tau = 30$ . The areas of the circles are proportional to the embedding times  $\tau_e$  employed in the reconstruction.

long autocorrelation times, so that causality is still detectable for large values of  $\tau$ . For this reason, the signals for the  $X \rightarrow Y$  link display a slow decay in the limit of large  $\tau$ . In the case of the coupled Rössler systems (Fig. 4a), this decay is convoluted with periodic oscillations which are not detected by the standard autocorrelation function (see SI) but are clearly visible in a statistical measure called distance autocorrelation [37, 38]. In particular, maxima in the distance autocorrelation of  $Y$  (see Fig. S4 in the SI) correspond to the minima of the blue curve in Fig. 4a, showing that the predictivity power of  $X(t)$  is degraded when  $Y(t)$  already carries much information about  $Y(t + \tau)$ . The reason why the space  $(\alpha X(t), Y(t))$  provides information about the state of  $Y$  in the past (say at time  $t - \tau$ ) is that, due to long-lasting time correlations, it carries memory of the state of the system in an even further past that already displayed the causal effect (say at time  $t - 2\tau$ ). Indeed, a constant coupling strength does not result into a single time-localized causal event, but generates a continuous influence of  $X$  on  $Y$ . In contrast, the green curves in Figs. 4a-b report the Imbalance Gains when we switched on the coupling  $X \rightarrow Y$  in the time window  $[0, 100]$  and set it to zero elsewhere. Since in these experiments the causal link is not present in the past, when we invert the order of cause and effect by taking negative values of  $\tau$  also its memory in the driver system is suppressed. As a consequence, causality is detected only for positive times, showing that the behaviour of this dynamical system is compatible with the first principle of Granger causality.

#### Robustness with respect to the embedding dimension.

In real-world applications, it is common to have access only to a limited number of dynamic variables from the systems that are tested for causality. In this case, the time-delay embedding approach becomes necessary. We investigated how

the Imbalance Gain is affected by the embedding parameters  $E$  and  $\tau_e$  on a pair of Lorenz 96 systems with  $F_X = 6$  and  $F_Y = 4$ , coupled in direction  $X \rightarrow Y$ . In Fig. 5 we show our causality measure in the direction without causal link ( $Y \rightarrow X$ ) for different choices of  $E$  (along the  $x$ -axis) and  $\tau_e$  (proportional to the area of the circles), restricting to a maximum window length  $(E - 1) \tau_e = 200$ . Each point was computed over 20 independent realizations, as described in the Methods section. Due to the absence of a causal link all the points should ideally lie on the dashed line (zero Imbalance Gain). According to Takens' theorem, when  $E$  is too small the time-delay embeddings do not provide a good representation of the full state space. In our measure this results into false positive detections for  $E \lesssim 10$ , which are particularly evident when the embedding time  $\tau_e$  is too large ( $\tau_e > 7$ , green circles). On the other hand, when  $E$  is sufficiently large and  $\tau_e$  is sufficiently small, the Imbalance Gain appears robust against the detection of spurious links for several different choices of the embedding parameters ( $\tau_e \leq 7$ , violet circles). In practical applications we suggest to fix  $\tau_e$  to a small value and compute  $\delta\Delta$  for increasing values of the embedding dimension  $E$ , considering the result reliable if its value reaches an approximate plateau. All the analysis shown in this work were performed following this criterion.

**Causality detection on EEG time series.** To benchmark our method on real-world time series we applied it to an unpublished EEG data set collected in our laboratories. In this experiment 19 healthy volunteers were asked to judge the duration of two stimuli, a visual and an auditory one, presented sequentially (see Methods - EEG experiment). Participants' task was to report, by pressing a key, which of the two stimuli was displayed for longer time. The first

stimulus in the pair, the comparison stimulus, was a visual grating varying randomly in display time (from 0.3 to 0.9 seconds) in each experimental trial. The second stimulus, called standard, was a burst of white noise presented through headphones for 0.6 seconds in each trial.

First we studied the causal link between the duration of the comparison stimulus and the EEG traces relative to its onset and its offset. Notably, in this application the driver variable is one-dimensional and time-independent. The Imbalance Gain was computed independently for each participant using the different trials as independent realizations and employing time-delay embeddings of 44 ms ( $E = 12$ ,  $\tau_e = 4$  ms). The results are shown in Fig. 6 for two example channels: one parieto-occipital (POz, panel a) and one frontal (Fz, panel b). We carried out two sets of measurements for different choices of the initial time  $t$  appearing in Eq. (2), which corresponds here to the first point of the predictive delay embedding. In the first tests we set  $t$  to the stimulus onset and we studied the behaviour of the Imbalance Gain  $\Delta(\alpha)$  as a function of the time lag  $\tau$ , limiting  $\tau$  to a window before the offset of the shortest stimulus. In this setting trials corresponding to different durations of the stimulus cannot be yet differentiated because the different compar-

ison stimuli are all indistinguishable in the time window considered; as a consequence, no coupling duration  $\rightarrow$  EEG activity should be observed. Consistently with this observation, we detected only a negligible information Imbalance Gain within the first 256 ms from stimulus onset (orange traces in Figs. 6a-b). Indeed, using a t statistics threshold for significant difference from zero of  $t = 2.552$  we found a total false positive rate of  $\sim 1.3\%$  across the channels. In the second set of tests we set the initial time  $t$  to the stimulus offset and we studied the Imbalance Gain within a window of 456 ms. From a perceptual stand point, this temporal window represents the period in which a signature of the subjective experience of stimulus duration should arise [39], because only after the offset of the stimulus its duration information becomes available to the participants. For this reason, we expected possible causal links to emerge. Using the same statistical procedure described above, we detected significant couplings with a different time modulation depending on the channel, whereby the Imbalance Gain started to raise at early latencies in occipital and parietal channels (see Fig. 6a and Fig. 6d) and peaked in a time span ranging from 300 to 400 ms after the stimulus offset also in frontal channels (see Fig. 6b and Fig. 6e). This result is in agree-

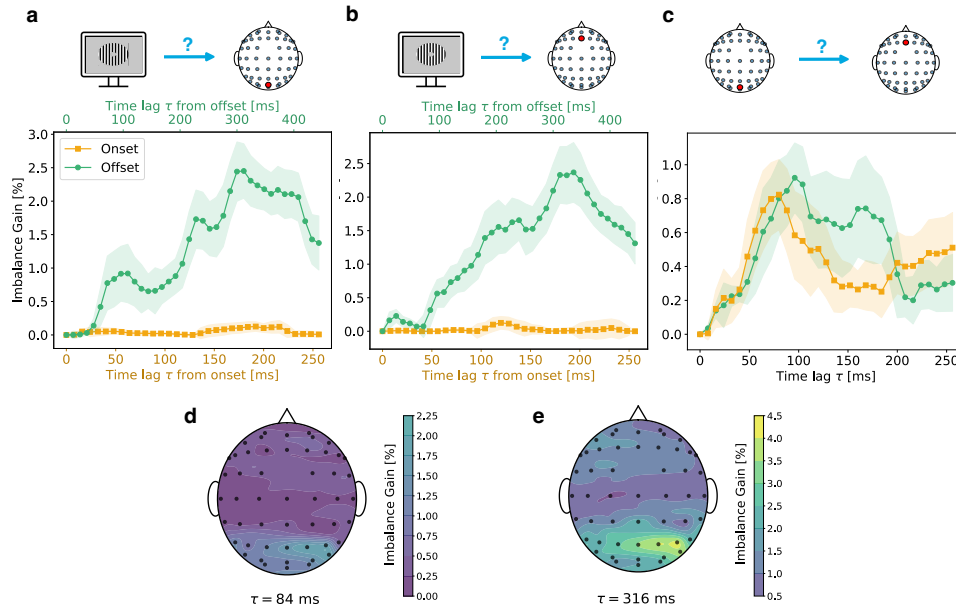


**Figure 6.** Imbalance Gains for the test  $(\alpha X(t), Y(t)) \rightarrow Y(t + \tau)$ , to assess the presence of the link from the duration of the stimulus and the EEG signals recorded by channels POz and Fz (panels a and b, respectively), and from channel POz to channel Fz (panel c). For the EEG signals, time-delay embeddings of length 44 ms were employed. The initial time  $t$  was set to the onset of the stimulus for the yellow curves, and to its offset for the green ones. The profiles were obtained by averaging the Imbalance Gains from 19 participants and the shaded area represent the standard error of this mean. The topoplots in panels d and e display the distributions of the Imbalance Gains for all the 51 channels tested, at two different time lags from the stimulus offset.



ment with recent EEG studies in the field of time perception which show that within similar latencies, and particularly in fronto-central electrodes, EEG activity contains information about participants’ perceived stimulus duration [40, 41]. As a comparison, we applied the Extended Granger Causality approach to the same causal detection task by optimizing its parameters independently from our tests (see Fig. S2 in the SI and the relative section for details). Using the Extended Granger Causality index we could observe only a faint signal after stimulus offset, and a total false positive rate of  $\sim 13.3\%$  after stimulus onset, around ten times more than with our approach.

Furthermore, we studied the causal relationships between two extremes of an hypothetical brain network functionally related to the processing of duration information. In this case the causal analysis was performed between two actual time series. Specifically, we evaluated the causal link between a parieto-occipital electrode, POz, and a fronto-central one, Fz. The activity of the former is supposedly linked with an early stage of duration processing [42] where stimulus sensory and duration information is encoded and conveyed to downstream brain regions (duration encoding), while the latter is associated to an higher-level processing stage where duration information is read out and used to perform the task at hand (duration decoding) [43]. This analysis was performed to assess whether our method is able to retrieve a signature of participants’ perceptual decision-making processes and its link to task performance. To this aim, we computed the Imbalance Gain POz  $\rightarrow$  Fz within 256 ms from stimulus’s comparison onset and offset (yellow and green traces in Fig. 6c), using time-delay embeddings of 44 ms for both the signals. We found that the Imbalance Gain relative to the different periods (i.e., onset or offset) changed differently as function of  $\tau$  (period, tau interaction:  $F_{26,468} = 1.529, p = 0.04$ ). In both periods the Imbalance Gain peaked around 90 ms, time lag which may reflect the propagation delay in the information flow between the two channels. However, in the onset period the signal slowly decayed until it reached a plateau, whereas after stimulus offset we observed a second peak in Imbalance Gain around  $\tau = 160$  ms. Interestingly, previous works have shown that, in the same electrode (Fz) and within similar latencies ( $\sim 150$  ms), it is possible to detect decision-related EEG activity which originates from feed-forward communication from the visual cortices [44, 45]. No such effect of the interaction between  $\tau$  and period on the Imbalance Gain was found in the case Fz  $\rightarrow$  POz ( $F_{26,468} = 0.448$ , see Fig. S5 in the SI). To better characterize the relationship between our results and participants’ performance we computed the Kendall’s correlation coefficient between the Imbalance Gain and participants’ accuracy in the task for each time lag  $\tau$  in each period. The result of this analysis showed that a positive

association is present only in the offset period in correspondence to the Imbalance Gain peaks (around 90 and 160 ms, see Fig. S6 in SI). Although more experiments are needed to further characterize the application of the Imbalance Gain in the field of neuroscience, these results clearly suggest that our method can provide a meaningful, model-free and interpretable metric to study both the causal relationship between the experimental manipulations and EEG activity and the connectivity between different EEG channels.

## Discussion

We proposed an approach to detect causality in time-ordered data based on Information Imbalance, a statistical measure constructed on distance ranks and interpretable within an information-theoretic framework. The underlying idea is to quantify how the description of a subset of variables in the future is affected by the addition of the putative causal variables in the past; in this sense, our method can be seen as a generalization of Granger causality, and alternative to measures such as the Transfer Entropy / Conditional Mutual Information.

We briefly discuss the main differences between Transfer Entropy and our method to outline the advantages of the latter. According to the information-theoretic formulation of our method (see SI), we assess the presence of the  $X \rightarrow Y$  link by evaluating a quantity which is a proxy of the Kullback–Leibler (KL) divergence:

$$\lim_{\eta \rightarrow 0} D_{KL} [p(R_{Y(t+\tau)} | R_{(\tilde{x}_{X(t), Y(t))} = \eta) } || p(R_{Y(t+\tau)})], \quad (4)$$

where  $R_{(\cdot)}$  are the random variables describing pairwise distances in the subscript space. For the same coupling direction, Transfer Entropy is defined as:

$$T_{x \rightarrow y} = D_{KL} [p(y_{t+1} | \tilde{x}_t, \tilde{y}_t) || p(y_{t+1} | \tilde{y}_t)]. \quad (5)$$

In Eq. (5)  $y$  identifies a single component of system  $Y$  (for instance  $y_1$ ), while  $\tilde{x}$  and  $\tilde{y}$  are time-delay embeddings. First, we observe that the distributions appearing in our KL divergence depend on the dynamic variables through distance functions constructed with those variables. This is relevant to reduce the dimensionality of the distributions to two, independently of the dimensionality of the underlying dynamics. Moreover, employing ranks allows computing a proxy of the KL divergence in a nonparametric fashion. Using distances rather than all the coordinates comes from the idea that only close copies in the past are relevant to predict the system state in the future. The constrain to small distances in the left conditional probability of Eq. (4) can be seen as an implementation of this idea, which is also at the basis of the estimate of Lyapunov exponents [46]. Furthermore, we notice that the KL divergence of our approach displays

a single conditional distribution, while the KL divergence appearing in Eq. (5) employs two conditionings. For this reason, Transfer Entropy directly contains the net effect of the causal variables on the effect ones, while we extract this information by comparing the KL divergence of Eq. (4) with the same object in absence of the causal variables, namely when the scaling parameter  $\alpha$  is set to zero.

In principle, a simpler criterion to the one proposed in this study is the occurrence of  $\Delta(X(t) \rightarrow Y(t + \tau)) < \Delta(Y(t) \rightarrow X(t + \tau))$  when the dominant causal link is  $X \rightarrow Y$ , and the occurrence of the opposite inequality when the  $Y \rightarrow X$  direction is the leading one. This method, which is equivalent to the measure  $L$  [28], faces the limitations illustrated in Fig. 3: the evaluation of a single inequality only allows to identify the dominant causal link, without recognizing situations where the coupling in one direction is absent.

The idea of re-defining the units of the dynamic variables by scaling them with optimal weights was already proposed in the Predictability Improvement approach [20]; here we simplified that idea by employing a single optimization parameter. Additionally, our method does not require any explicit prediction rule and exploits the maximal information available - in the spaces of time-delay embeddings - not only in the past frame where the prediction is made, but also in the future frame where the quality of the prediction is assessed. Predictability Improvement, in contrast, computes prediction errors in the low-dimensional spaces of the variables used for state space reconstruction (see SI).

We tested our method on several coupled dynamical systems with different coupling configurations featuring both unidirectional and bidirectional links. In case of missing dynamic variables, our measure can be applied with time-delay embeddings, although their use can be seen as an optional feature rather than a requirement of the method. We observed that the Imbalance Gain allows a robust detection of causal links in each direction and provides a ranking of the coupling strengths of different processes. Even though not immune to false positives, our measure appears significantly more robust than the compared methods against this drawback, especially in the high-dimensional scenario. Additionally, we observed that the results are stable up to a significant level of additive noise (see Fig. S1 in the SI) and robust against data downsampling (see Fig. S7 in the SI). When the only purpose of the test is assessing the presence or absence of the causal link, the Imbalance Gain provides stable results against different choices of the time lag  $\tau$ . As a rule of thumb, we suggest to choose  $\tau$  smaller than the decay time of the distance autocorrelation function of the putative driven system, if it displays no oscillations, or in correspondence of its first minimum otherwise. Importantly, in case of partial knowledge of the dynamical variables this corre-

lation measure can be still computed in the reconstructed state space (see SI). As for other causality measures employing time-delay embeddings, the outcome of our method is affected by the choice of the embedding parameters. We showed that when  $\tau_e$  is small enough (in the order of one or two sampling times in all the time series that we tested), the Imbalance Gain statistically converges to zero as a function of the embedding length in the direction without any dynamical coupling. This provides a straightforward procedure to assess whether a weak causal link is spurious or absent.

We further applied our measure to real-world time series from EEG experiments, studying the time modulation of causal links from an experimental and static variable - the duration of the comparison stimulus - to the channel-dependent EEG activity, and between EEG activities of different channels. The null tests conducted after the stimulus onset in the former case confirmed the method's robustness against the detection of spurious causalities. In the tests uncovering causal signals, the time modulations of the Imbalance Gain appear consistent with the latencies at which the information of stimulus duration is expected to be transferred from the visual cortex to the fronto-central channels and elaborated by the latter. Additionally, the tests revealed that our causality measure can be easily linked with participants performance. Our findings suggest that applying our approach to *ad hoc* experiments may provide new insights into inferring functional brain connectivity.

In conclusions, we introduced an approach which allows inferring the presence of causal links in dynamical processes. Even if the zoo of methods aimed at the same task is crowded, we believe that the benchmark presented in this work demonstrate that this approach overcomes some of the limitations of other model-free approaches. Its stronger statistical power shows up in particular when applied to high-dimensional systems in which *causality is absent*, a scenario which is of the utmost important for understanding how to control a system. This, we believe, will trigger the interest of scientists working on causality detection in real-world time-dependent data.

## Methods

**Dynamical systems.** The dynamical systems employed for the tests are based on a first-order dynamics that can be generally written as

$$\dot{X} = f(X) \tag{6a}$$

$$\dot{Y} = g(Y) + \varepsilon G(X, Y) \tag{6b}$$

in the case of unidirectional coupling ( $X \rightarrow Y$ ), and

$$\dot{X} = f(X) + \varepsilon_{Y \rightarrow X} F(X, Y) \tag{7a}$$

$$\dot{Y} = g(Y) + \varepsilon_{X \rightarrow Y} G(X, Y) \tag{7b}$$

in the case of bidirectional coupling ( $X \leftrightarrow Y$ ). In the unidirectional setting we tested two Rössler systems both with identical frequencies ( $\omega_1 = \omega_2 = 1.1015$ ) and with different frequencies ( $\omega_1 = 1.1015$ ,  $\omega_2 = 0.985$ , as studied in [24] and [36]), and two 40-dimensional Lorenz 96 systems with different forcing constants ( $F_X = 5$  and  $F_Y = 6$  in Fig. 3 and Fig. 4,  $F_X = 6$  and  $F_Y = 4$  in Fig. 5). We tested the bidirectional scenario using two identical Rössler systems with the same parameters reported above, and two identical Lorenz systems with parameters  $\sigma = 10$ ,  $\beta = 8/3$  and  $\rho = 28$ . All the tests were performed by extracting from the trajectories  $N = 5000$  realizations, except for the Convergent Cross Mapping method that requires to monitor the convergence of the results as a function of the trajectory length. All the dynamical systems were integrated using the 8-th order explicit Runge-Kutta method DOP853 in the Python library SciPy, except for the coupled Lorenz 96 systems for which the SciPy implementation of the LSODA integrator was employed [47]. We refer to the SI for the explicit equations of each pair of systems.

**Average Imbalance Gain.** In the tests as a function of the embedding parameters and in the analysis to the EEG activity we repeatedly applied our causality measure to independent realizations of the same dynamical process (trajectories starting from different initializations for the Lorenz 96 systems and experiments over different participants in the EEG application). In both the cases the average Imbalance Gain was computed by maximizing the average  $\alpha$ -dependent Imbalance Gain  $\langle (\Delta(\alpha = 0) - \Delta(\alpha)) / \Delta(\alpha = 0) \rangle$ , where the brackets identify the average across different realizations. With this procedure a single optimal scaling parameter was inferred for all the realizations.

**EEG experiment.** Nineteen healthy volunteers took part in this experiment (mean age: 24.10, SD: 3.43, 8 females). All volunteers gave written informed consent to participate to this study, the procedures of which were approved by the International School for Advanced Studies (SISSA) ethics committee in accordance with the Declaration of Helsinki. Volunteers underwent six experimental blocks, each composed by 60 trials. In each trial, a visual stimulus, varying in display time trial by trial, was presented at the center of the screen (Samsung 22" SyncMaster 2233RZ, 1680x1050 pixels resolution, 120 Hz refresh rate, viewing distance 60 cm, grey background color). This stimulus, called comparison, was a sinusoidal annulus grating (5 degrees of visual angle outer-circle diameter, 1 degree of visual angle inner-circle diameter, 1 cycle per degree, 100% contrast) composed by 5 concentric parts of equal area slowly and rigidly rotating around the center of the screen ( $\sim 0.6$  rad/s with alternating rotation senses, either clockwise or counterclockwise). The comparison stimulus could be displayed for 0.3, 0.4,

0.5, 0.6, 0.7, 0.8 or 0.9 seconds in each trial and it was followed (after an interval uniformly distributed between 0.5 and 1 second) by an auditory stimulus of 0.6 seconds (burst of white noise delivered through Etymotic Research ER1 Insert Earphones). Each stimulus duration was tested 10 times in each block. Volunteers were instructed to maintain their gaze on a fixation cross (0.2 degrees of visual angle in diameter) presented at the center of the screen throughout the experiment and to report, by pressing a button on the keyboard, whether the first or the second stimulus was presented for longer time. After providing the response the next trial started automatically after an interval uniformly distributed between 0.5 and 1 second. Volunteers received no feedback on their performance. Volunteers performed the task comfortably sitting in front of the apparatus while we recorded their EEG activity using 64 active electrodes Brain-Products actiCHamp Plus (Brain Products GmbH, Gilching, Germany) with 2048 Hz sampling frequency. In order to minimize head motion and blink artifacts, volunteers placed their head on a chin rest and they were instructed to blink when providing the response. EEG data preprocessing was performed using EEGLAB toolbox [48] in Matlab (Mathworks Inc.). First, we removed motion and blink artifacts using automatic labeling of independent components (IC) using the ICLabel toolbox [49]. Only ICs with a probability higher than 90% of being correctly classified as muscle or eye artifact were removed. Then, the continuous EEG signal was downsampled to 250 Hz sampling rate, referenced to a common average reference and filtered using a 4<sup>th</sup>-order Butterworth band-pass filter with range 0.1-40 Hz. The EEG data corresponding to the comparison stimulus was epoched starting from 200 ms before its onset to 500 ms after its offset. These epochs were detrended, and were examined to remove any remaining artifacts. We automatically removed epochs based on signal amplitude threshold, removing all trials in which the EEG amplitude exceeded  $\pm 50 \mu\text{V}$ . All the remaining trials were visually inspected to detect and remove the ones containing any residual artifacts. A total of  $\sim 0.1\%$  of trials were discarded. Additionally, we excluded from further analyses temporal channels (T7, T8, TP7, TP8, TP9, TP10, P7, P8, FT7, FT8, FT9, FT10). We constructed then two data sets corresponding to the onset and offset period of comparison presentation, available at the link reported in the Data availability Section. The onset data set contained EEG traces of 300 ms length starting from stimulus onset baseline corrected using 44 ms pre-stimulus period. The offset data set consisted of EEG traces of 500 ms length starting from stimulus offset baseline corrected using the 88 ms window centered at stimulus offset (44 ms pre-offset and 44 ms post-offset period). Statistical assessment on Imbalance Gain data was performed using SciPy [47] and statsmodels [50] packages in Python. In particular

we performed a repeated measures ANOVA to understand the effect of the time lag  $\tau$  and the period (i.e., onset and offset) on the Imbalance Gain in the case  $\text{POz} \rightarrow \text{Fz}$  and  $\text{Fz} \rightarrow \text{POz}$ . This analysis was performed using *AnovaRM* function with  $\tau$  and period as within-subjects factors, considering only values of  $\tau$  larger than 44 ms in order to avoid any overlap between the time-delay embeddings at time 0 and time  $\tau$ .

**Extended Granger causality.** We implemented the method as described in Ref. [16], performing local linear regressions in the joint shadow manifold of  $x_1$  and  $y_1$  within neighborhoods of 200 randomly selected points. The size of the neighborhoods was kept constant for all the coupling strengths of each pair of systems, and quantified in terms of the number  $k$  of neighbors instead of using the radius  $\delta$ . We found this useful to better control the neighborhood size and fix it to small values, where this method is expected to reveal the true causal relations when the underlying dynamics is nonlinear [16]. We chose  $k$  using a single experiment at fixed  $\varepsilon$  for each pair of systems, and then we used it to compute the extended Granger causality index for all the experiments. We repeated these steps for several choices of the time-delay embedding parameters, selecting the combination with outcome signals more in agreement with the ground truth coupling. With this procedure we set  $k = 200$ ,  $E = 3$  and  $\tau_e = 1$  both for the Rössler systems and the Lorenz ones, and we chose  $k = 500$ ,  $E = 30$  and  $\tau_e = 7$  for the Lorenz 96 systems.

**Convergent Cross Mapping.** The method was implemented as described in Ref. [7], using neighborhoods of size  $E + 1$  in the shadow manifolds of  $x_1$  and  $y_1$  to compute the cross mapping coefficients. The cross-map skill, quantified by the Pearson correlation  $\rho$  between the reconstructed and the ground-truth points in spaces  $x_1$  and  $y_1$ , was studied as a function of the length  $L$  of the trajectory in order to select  $\rho$  after convergence. In particular, we observed convergence at  $L = 30000$  for the identical Rössler systems ( $E = 3$ ,  $\tau_e = 5$ ),  $L = 20000$  for the different Rössler systems ( $E = 3$ ,  $\tau_e = 5$ ),  $L = 40000$  for the bidirectionally coupled Lorenz systems ( $E = 3$ ,  $\tau_e = 3$ ) and  $L = 50000$  for the Lorenz 96 systems ( $E = 30$ ,  $\tau_e = 7$ ). The optimal values of  $\tau_e$  were observed in correspondence of the first minimum of the mutual information [32].

**Measure  $L$ .** We applied this method following Ref. [28]. Also in this case the optimal values of  $\tau_e$  were chosen accordingly to the mutual information criterion, except for the case of the Lorenz 96 systems, where we found  $\tau_e = 1$  to minimize the difference between the signals in the  $X \rightarrow Y$  and  $Y \rightarrow X$  couplings, ranked anyway in the wrong order. We set  $k = 5$  both for the Rössler and the Lorenz systems,

and  $k = 20$  for the Lorenz 96 systems.

## Data availability

The EEG data analyzed in this study are available at <https://osf.io/6jpvvg/>.

## Code availability

Supporting codes are available at the GitHub repository <https://github.com/vdeltatto/imbalance-gain-causality.git>. The repository also contains the codes to generate the trajectories of the dynamical systems analyzed in this work. The Information Imbalance measure is also implemented in the Python package DADapy [51].

## References

- [1] N. Altman and M. Krzywinski. “Association, correlation and causation”. *Nat. Methods* **12**, 899-900 (2015).
- [2] P. Spirtes and K. Zhang. “Causal discovery and inference: concepts and recent methodological advances”. *Appl. Inform.* **3**, 1–28 (2016).
- [3] G. Gendron, M. Witbrock, and G. Dobbie. *A Survey of Methods, Challenges and Perspectives in Causality*. 2023.
- [4] C. W. J. Granger. “Investigating Causal Relations by Econometric Models and Cross-spectral Methods”. *Econometrica* **37**, 424–438 (1969).
- [5] J. Pearl. *Causality: Models, Reasoning and Inference*. Cambridge University Press, 2009.
- [6] K. D. Hoover. “Causality in Economics and Econometrics”. *The New Palgrave Dictionary of Economics*. Palgrave Macmillan UK, 2017.
- [7] G. Sugihara et al. “Detecting Causality in Complex Ecosystems”. *Science* **338**, 496-500 (2012).
- [8] M. Kretschmer et al. “Using Causal Effect Networks to Analyze Different Arctic Drivers of Midlatitude Winter Circulation”. *J. Clim.* **29**, 4069 - 4081 (2016).
- [9] K. Friston, L. Harrison, and W. Penny. “Dynamic causal modelling”. *NeuroImage* **19**, 1273-1302 (2003).
- [10] M. Kaminski et al. “Evaluating causal relations in neural systems: Granger causality, directed transfer function and statistical assessment of significance”. *Biol. Cybern.* **85**, 145-157 (2001).
- [11] S. L. Bressler and A. K. Seth. “Wiener–Granger Causality: A well established methodology”. *NeuroImage* **58**, 323-329 (2011).

- [12] J. Runge. “Causal network reconstruction from time series: From theoretical assumptions to practical estimation”. *Chaos* **28** (2018).
- [13] J. Runge et al. “Inferring causation from time series in Earth system sciences”. *Nat. Comm.* **10**, 2553 (2019).
- [14] A. E. Yuan and W. Shou. “Data-driven causal analysis of observational biological time series”. *eLife* **11**, e72518 (2022).
- [15] E. Beckenbach. *N. Wiener, in: Modern Mathematics for Engineers. The Science of Microfabrication*. McGraw-Hill, New York, 1956.
- [16] Y. Chen et al. “Analyzing multiple nonlinear time series with extended Granger causality”. *Phys. Lett. A* **324**, 26-35 (2004).
- [17] D. Marinazzo, M. Pellicoro, and S. Stramaglia. “Non-linear parametric model for Granger causality of time series”. *Phys. Rev. E* **73**, 066216 (2006).
- [18] D. Marinazzo, M. Pellicoro, and S. Stramaglia. “Kernel Method for Nonlinear Granger Causality”. *Phys. Rev. Lett.* **100**, 144103 (2008).
- [19] L. Barnett and A. K. Seth. “Granger causality for state-space models”. *Phys. Rev. E* **91**, 040101 (2015).
- [20] A. Krakovská and F. Hanzely. “Testing for causality in reconstructed state spaces by an optimized mixed prediction method”. *Phys. Rev. E* **94**, 052203 (2016).
- [21] M. Wang and Z. Fu. “A new method of nonlinear causality detection: Reservoir computing Granger causality”. *Chaos Solitons & Fractals* **154**, 111675 (2022).
- [22] T. Schreiber. “Measuring Information Transfer”. *Phys. Rev. Lett.* **85**, 461–464 (2000).
- [23] M. Paluš et al. “Synchronization as adjustment of information rates: Detection from bivariate time series”. *Phys. Rev. E* **63**, 046211 (2001).
- [24] M. Paluš and M. Vejmelka. “Directionality of coupling from bivariate time series: How to avoid false causalities and missed connections”. *Phys. Rev. E* **75**, 056211 (2007).
- [25] L. Barnett, A. B. Barrett, and A. K. Seth. “Granger Causality and Transfer Entropy Are Equivalent for Gaussian Variables”. *Phys. Rev. Lett.* **103**, 238701 (2009).
- [26] J. Runge et al. “Escaping the Curse of Dimensionality in Estimating Multivariate Transfer Entropy”. *Phys. Rev. Lett.* **108**, 258701 (2012).
- [27] F. Takens. “Detecting strange attractors in turbulence”. *Dynamical Systems and Turbulence, Warwick 1980*. Ed. by D. Rand and L.-S. Young. Springer Berlin Heidelberg, 1981.
- [28] D. Chicharro and R. G. Andrzejak. “Reliable detection of directional couplings using rank statistics”. *Phys. Rev. E* **80**, 026217 (2009).
- [29] E. N. Lorenz. “Atmospheric Predictability as Revealed by Naturally Occurring Analogues”. *J. Atmos. Sci.* **26**, 636 - 646 (1969).
- [30] A. Glielmo et al. “Ranking the information content of distance measures”. *PNAS Nexus* **1** (2022). pgac039.
- [31] T. Cover and J. Thomas. *Elements of Information Theory*. Wiley, 2012.
- [32] A. M. Fraser and H. L. Swinney. “Independent coordinates for strange attractors from mutual information”. *Phys. Rev. A* **33**, 1134–1140 (1986).
- [33] M. B. Kennel, R. Brown, and H. D. I. Abarbanel. “Determining embedding dimension for phase-space reconstruction using a geometrical construction”. *Phys. Rev. A* **45**, 3403–3411 (1992).
- [34] A. Krakovská et al. “State space reconstruction techniques and the accuracy of prediction”. *Commun. Nonlinear Sci. Numer. Simul.* **111**, 106422 (2022).
- [35] D. Coufal et al. “Detection of coupling delay: A problem not yet solved”. *Chaos* **27**, 083109 (2017).
- [36] M. Paluš et al. “Causality, dynamical systems and the arrow of time”. *Chaos* **28**, 075307 (2018).
- [37] G. J. Székely, M. L. Rizzo, and N. K. Bakirov. “Measuring and testing dependence by correlation of distances”. *Ann. Stat.* **35**, 2769 – 2794 (2007).
- [38] C. F. O. Mendes, R. M. da Silva, and M. W. Beims. “Decay of the distance autocorrelation and Lyapunov exponents”. *Phys. Rev. E* **99**, 062206 (2019).
- [39] T. W. Kononowicz and H. van Rijn. “Decoupling Interval Timing and Climbing Neural Activity: A Dissociation between CNV and N1P2 Amplitudes”. *J. Neurosci.* **34**, 2931 - 2939 (2014).
- [40] N. Ofir and A. N. Landau. “Neural signatures of evidence accumulation in temporal decisions”. *Curr. Biol.* **32**, 4093-4100.e6 (2022).
- [41] A. Damsma, N. Schlichting, and H. van Rijn. “Temporal Context Actively Shapes EEG Signatures of Time Perception”. *J. Neurosci.* **41**, 4514–4523 (2021).
- [42] Y. Tonoyan et al. “Subjective time is predicted by local and early visual processing”. *NeuroImage* **264**, 119707 (2022).

- [43] F. Protopapa et al. “Topographic Connectivity in a Duration Selective Cortico-Cerebellar Network”. *bioRxiv* (2020).
- [44] S. Thorpe, D. Fize, and C. Marlot. “Speed of Processing in the Human Visual System”. *Nature* **381**, 520-2 (1996).
- [45] M. Fabre-Thorpe et al. “A Limit to the Speed of Processing in Ultra-Rapid Visual Categorization of Novel Natural Scenes”. *J. Cogn. Neurosci.* **13**, 171-180 (2001).
- [46] A. Wolf et al. “Determining Lyapunov exponents from a time series”. *Physica D* **16**, 285-317 (1985).
- [47] P. Virtanen et al. “SciPy 1.0: Fundamental Algorithms for Scientific Computing in Python”. *Nat. Methods* **17**, 261–272 (2020).
- [48] A. Delorme and S. Makeig. “EEGLAB: an open source toolbox for analysis of single-trial EEG dynamics including independent component analysis”. *J. Neurosci. Methods* **134**, 9-21 (2004).
- [49] L. Pion-Tonachini, K. Kreutz-Delgado, and S. Makeig. “ICLabel: An automated electroencephalographic independent component classifier, dataset, and website”. *NeuroImage* **198**, 181-197 (2019).
- [50] S. Seabold and J. Perktold. “Statsmodels: Econometric and statistical modeling with python”. *9th Python in Science Conference*. 2010.
- [51] A. Glielmo et al. “DADapy: Distance-based analysis of data-manifolds in Python”. *Patterns* **3**, 100589 (2022).

## Acknowledgments

We would like to thank Prof. Ali Hassanali and Dr. Michele Allegra for providing useful comments and insights and Dr. Yelena Tonoyan for contributing to EEG data collection and preprocessing.

**Supplementary Information for**

**Robust inference of causality in high-dimensional dynamical processes from the  
Information Imbalance of distance ranks**

Vittorio Del Tatto<sup>1</sup>, Gianfranco Fortunato<sup>1</sup>, Domenica Bueti<sup>1</sup>, and Alessandro Laio<sup>1,2</sup>

<sup>1</sup> Scuola Internazionale Superiore di Studi Avanzati, SISSA, via Bonomea 265, 34136 Trieste, Italy

<sup>2</sup> ICTP, Strada Costiera 11, 34151 Trieste, Italy

## Information-theoretic formulation of the method

### Copula variables

The bridge between the Information Imbalance measure and information theory rests on the statistical theory of copulas. Given a two-dimensional random variable  $\mathbf{R} = (R_A, R_B)$  with joint density  $p_{AB}(R_A, R_B)$  and marginal densities  $p_A(R_A)$ ,  $p_B(R_B)$ , we define its *copula variable* as

$$\mathbf{C} = (c_A, c_B) = (F_A(R_A), F_B(R_B)), \quad (8)$$

where  $F_A$  is the cumulative distribution of  $R_A$ :  $F_A(R) = \int_{-\infty}^R dR' p_A(R')$  (similarly for  $F_B$ ). The relevance of copula variables lies in the two following results:

- the marginals of  $\mathbf{C}$  are uniformly distributed in  $[0, 1]$ , result known as *probability integral transform* [1]:

$$c_A \sim U_{[0,1]}, \quad c_B \sim U_{[0,1]}; \quad (9)$$

- according to Sklar's theorem [2], the joint density of  $\mathbf{R}$  can be decomposed as the product of the marginal densities and a joint copula distribution:

$$p_{AB}(R_A, R_B) = \tilde{p}_{AB}(c_A, c_B) p_A(R_A) p_B(R_B). \quad (10)$$

Given these properties, it is possible to show that the mutual information between variables  $R_A$  and  $R_B$  can be expressed equivalently as the conditional entropy of their copulas [3, 4]:

$$I(R_A, R_B) = -H(c_A | c_B) = -H(c_B | c_A). \quad (11)$$

### Information Imbalance as a KL divergence

Let's consider a data set  $\{x_i\}_{i=1}^N$  harvested from a density  $p(x)$  defined over an embedding manifold  $M$ , provided with two distance measures  $d_A$  and  $d_B$ . Calling  $R_A$  and  $R_B$  the RVs describing the pair-wise distances between the points, their realizations compose two sets  $\{R_{ij}^A\}$  and  $\{R_{ij}^B\}$  ( $i, j = 1, \dots, N$  with  $i \neq j$ ). The realizations of the corresponding copula variables  $c_A$  and  $c_B$  define the collections  $\{\frac{1}{N}r_{ij}^A\}$  and  $\{\frac{1}{N}r_{ij}^B\}$ , where  $r_{ij}^A$  and  $r_{ij}^B$  are the ranks of point  $j$  relative to point  $i$  according to the two metrics, as defined in the main text. Then, distance ranks and copulas are statistically identical variables. Starting from Eq. (11) it was shown in [5] that Information Imbalance emerges as the proxy of an information-theoretic object, namely

$$\Delta(d_A \rightarrow d_B) \approx 2 \exp \left( -\frac{\partial}{\partial h} I^h(d_A \rightarrow d_B) |_{h=0} - 1 \right), \quad (12)$$

where  $I^h$  denotes a *restricted mutual information* over one of the two integration intervals:

$$I^h(d_A \rightarrow d_B) = - \int_0^h d\tilde{c}_A H(c_B | c_A = \tilde{c}_A). \quad (13)$$

Eq. (12) is derived under two assumptions, i.e. supposing that the conditional distribution of copulas  $p(c_B | c_A = \varepsilon)$  is closely peaked around zero in the limit  $\varepsilon \rightarrow 0$ , and that it can be modelled as an exponential. We can further develop this quantity aiming to obtain a more interpretable object:

$$\frac{\partial}{\partial h} I^h(d_A \rightarrow d_B) |_{h=0} = - \lim_{\varepsilon \rightarrow 0} H(c_B | c_A = \varepsilon) \quad (14a)$$

$$= \lim_{\varepsilon \rightarrow 0} \int_0^1 dc_B p(c_B, c_A = \varepsilon) \log p(c_B, c_A = \varepsilon), \quad (14b)$$

where in the last passage we used that  $c_A \sim U_{[0,1]}$ . Then, applying Sklar's theorem and defining  $\eta = F_A^{-1}(\varepsilon)$  we can re-write the last integral using the distance variables  $R_A$  and  $R_B$ :

$$(14) = \lim_{\eta \rightarrow 0} \int_0^{+\infty} dR_B p(R_B | R_A = \eta) \log \frac{p(R_B | R_A = \eta)}{p(R_B)} \quad (15a)$$

$$= \lim_{\eta \rightarrow 0} D_{KL}[p(R_B | R_A = \eta) \| p(R_B)], \quad (15b)$$



where  $D_{KL}$  denotes the Kullback-Leibler divergence, which is a pseudodistance between probability distributions. Finally, replacing in Eq. (12) we find

$$\Delta(d_A \rightarrow d_B) \approx 2 \exp \left( - \lim_{\eta \rightarrow 0} D_{KL} [p(R_B | R_A = \eta) \| p(R_B)] - 1 \right). \quad (16)$$

Eq. (16) formalizes the idea of informativeness among distance spaces: when we condition the distribution of distances in  $d_B$  to close points according to  $d_A$ , the greater the change in the distribution, the more informative  $d_A$  is considered to be with respect to  $d_B$ . Specializing Eq. (16) to the distance spaces  $A = (\alpha X(t), Y(t))$  and  $B = Y(t + \tau)$ , the optimization over  $\alpha$  takes the form of a *minimum entropy* protocol, where we aim to maximize the predictability of the future distances in the space of the effect variable when we consider points that were close in the past according to both the effect and the causal variables.

## Connection with measure L

In [6], Chicharro and Andrzejak introduced a rank-based measure to detect unidirectional couplings in non-synchronizing conditions, lying on the idea of state space reconstruction using time-delay embeddings. Given the one-dimensional time series  $x(t)$  and  $y(t)$  ( $t = 1, \dots, N$ ) and their time-delay embeddings  $\tilde{x}(t)$  and  $\tilde{y}(t)$ , we call  $v_{tj}$  and  $w_{tj}$  the time indices of the  $j$ -th nearest neighbors of  $\tilde{x}(t)$  and  $\tilde{y}(t)$ , respectively, from which we exclude temporal neighbors within a window of size  $W$  ( $|v_{tj} - t| \leq W$  and  $|w_{tj} - t| \leq W$ ). Distances are measured in the time-delay spaces with the Euclidean metric, denoted in the following as  $d_X$  and  $d_Y$ . Considering  $k$  nearest neighbors for each point, the *measure L* is defined as

$$L(X | Y) = \frac{1}{N} \sum_{t=1}^N \frac{G_t(X) - G_t^k(X | Y)}{G_t(X) - G_t^k(X)}, \quad (17)$$

where  $G_t(X)$ ,  $G_t^k(X)$  and  $G_t^k(X | Y)$  are respectively the mean rank, the minimal mean rank and the  $Y$ -conditioned mean rank:  $G_t(X) = \frac{N}{2}$ ,  $G_t^k(X) = \frac{k+1}{2}$  and  $G_t^k(X | Y) = \frac{1}{k} \sum_{j=1}^k r_{t,w_{tj}}$ . Taking only the first nearest neighbor ( $k = 1$ ), it is easy to show that the measure  $L$  is related to the standard Information Imbalance by a straightforward linear relation:

$$L(X | Y) = \frac{1}{N} \sum_{t=1}^N \frac{N/2 - G_t^1(X | Y)}{N/2 - 1} \quad (18a)$$

$$= \frac{N}{N-2} - \frac{2}{N-2} \frac{1}{N} \sum_{t=1}^N G_t^1(X | Y) \quad (18b)$$

$$= \frac{N}{N-2} - \frac{2}{N-2} \langle r_X | r_Y = 1 \rangle \quad (18c)$$

$$= \frac{N}{N-2} [1 - \Delta(Y \rightarrow X)]. \quad (18d)$$

Using a generic number of neighbors  $k$ , this relation becomes

$$L(X | Y) = \frac{N}{N-k-1} [1 - \Delta(Y \rightarrow X; k)]. \quad (19)$$

We notice that the Information Imbalance of Eq. (18d) is referred to distance spaces with no relative time lag ( $\tau = 0$ ), which is a relevant difference between state space reconstruction methods such as the measure  $L$  and methods based on predictability. In [6] the authors proposed to assess the presence of the coupling  $X \rightarrow Y$  by checking whether the condition  $\Delta L = L(X | Y) - L(Y | X) > 0$  is verified. In terms of the Information Imbalance measure, this translates into the inequality  $\Delta(Y \rightarrow X) < \Delta(X \rightarrow Y)$ .

## Comparison with Predictability Improvement

Predictability Improvement was introduced in Ref. [7] as a method generalizing the predictivity criterion of Granger causality and working in the spaces of time-delay embeddings  $M_X \ni \tilde{x}$  and  $M_Y \ni \tilde{y}$ , constructed from the one-dimensional components  $x$  and  $y$  of the unknown dynamical systems  $X$  and  $Y$ . To study the presence of the  $X \rightarrow Y$  coupling, the authors proposed the following pipeline:

1. Randomly sample  $N$  time indices from the trajectory.
2. For each sample  $y_t$ , make a prediction  $\widehat{y}_{t+1}$  of the next one-dimensional state  $y_{t+1}$  by means of a rule generalizing the method of analogues [8], which keeps into account the  $k$  closest states in the past trajectory:

$$\widehat{y}_{t+1} = \sum_{h=1}^k \frac{w_h}{\sum_{h'=1}^k w_{h'}} (y_t + y_{t_{h+1}} - y_{t_h}). \quad (20)$$

Here  $t_h < t$  denotes the time index of the  $h$ -th nearest neighbor in the previous history of the system, according to Euclidean distances in the  $M_Y$  space. The weights  $w_h$  take the form

$$w_h = \exp\left(-\frac{\|\widetilde{y}_t - \widetilde{y}_{t_h}\|}{\min_{h'} \|\widetilde{y}_t - \widetilde{y}_{t_{h'}}\|}\right) \quad (21)$$

and they exponentially decrease the relevance of neighbors in the prediction rule with their distance from the central point.

3. For each prediction compute the residual  $e_{t+1} = y_{t+1} - \widehat{y}_{t+1}$ .
4. Repeat points 2 and 3 but measuring distances in the space  $M_{XY}$ , where the time-delay embedding with index  $t$  is a concatenation of  $\widetilde{x}_t$  and  $\widetilde{y}_t$ . This brings to new predictions  $\widehat{y}_{t+1}^X$  and new residuals,  $e_{t+1}^X = y_{t+1} + \widehat{y}_{t+1}^X$ .
5. Perform a statistical test to assess if  $\text{Var}(e^X) < \text{Var}(e)$ . If the inequality is statistically satisfied,  $X$  causes  $Y$ .

The method reckons on time-delay embeddings featuring a scaling parameter for each component; these weights should be optimized to reach the lowest possible residuals. According to the Ref. [7], this multidimensional optimization is necessary to avoid the natural increase of the residuals  $e^X$  that would occur only as a consequence of the decreased density of points in space  $M_{XY}$  compared to space  $M_Y$ .

One of main differences of our approach is that it does not require any explicit prediction of the state of the putative driver in the future. This becomes more evident if we restrict to the case  $k = 1$  and we write the one-point residual computed by the Predictability Improvement approach - e.g. using distances computed in  $M_Y$  - as

$$e_{t+1} = (y_{t+1} - y_{t_1}) - (\widehat{y}_{t+1} - y_{t_1}). \quad (22)$$

By employing distance ranks, the implicit prediction in our approach is that if  $\widetilde{y}_t$  and  $\widetilde{y}_{t_1}$  are nearest neighbor, their time-evolved versions  $\widetilde{y}_{t+1}$  and  $\widetilde{y}_{t_1+1}$  will still be nearest neighbors. This allows us not to explicitly consider the second term of Eq. (22), because it would trivially correspond to an expected conditional rank equal to 1 for all the point-wise predictions. In our measure, the first term of Eq. (22) is replaced by the rank of point  $\widetilde{y}_{t+1}$  with respect to point  $\widetilde{y}_{t_1+1}$ . We notice that the difference does not lie only in the use of rank distances, but also in the fact that in the future frame we still compute distances in the reconstructed state space  $M_Y$ , instead of considering the original one-dimensional signals to assess the quality of the prediction. Indeed, the proximity of points  $\widetilde{y}_{t+1}$  and  $\widetilde{y}_{t_1+1}$  could be not well represented by the single components  $y_{t+1}$  and  $y_{t_1+1}$ , especially when the embedding dimension is large.

## Stability with respect to noise

We carried out two sets of measurements, the former where noise is added *a posteriori* to the deterministic trajectory and interpreted as a result of measurement errors (Fig. S1a), and the latter where it comes from an underlying stochastic dynamics (Fig. S1b), namely it is added at each integration step. To avoid mixing the effect of noise with other nuisance sources, we computed the Imbalance Gain considering all the coordinates of the two systems. As expected, in both scenarios the signal in the  $X \rightarrow Y$  direction appears to weaken as the noise level increases. Concerning the link  $Y \rightarrow X$ , the signal is negligible up to a 15 % noise level in the first case (Fig. S1a), while the Imbalance Gain remains close to zero for all the tested noise amplitudes in the second scenario. We interpret this difference as follows. When the noise is added a posteriori on a deterministic signal, its effect is to reduce the information content of the space  $d_{X(0)}$  with respect to  $d_{X(\tau)}$ , so that the former is not anymore the most informative that one can build with the dynamic variables at time 0. As a consequence, part of the information which is lost is recovered when the driven system  $Y(0)$  is added to this space as tuned by the parameter  $\alpha$ , resulting in a nonzero Imbalance Gain. In a stochastic dynamics, instead, the effect of noise is to reduce the predictability of  $X(\tau)$  given the knowledge of  $X(0)$ ; however, the space  $d_{X(0)}$  remains the most informative that one can construct with the dynamic variables at time 0.

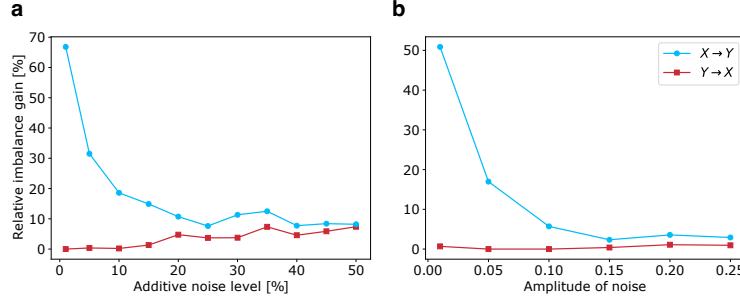


**Figure S1.** Effect of noise on the Imbalance Gain, measured on the unidirectionally coupled Rössler systems ( $X \rightarrow Y$ ) with coupling  $\varepsilon = 0.1035$ . **a)** White noise was added a posteriori and independently to each dynamical variable, choosing its amplitude as a fraction (along the  $x$ -axis) of the standard deviation of the entire trajectory in the corresponding direction. **b)** Independent white noises were added during the integration of the dynamical systems, only to the variables  $x_1$  and  $y_1$ , with amplitude reported along the  $x$ -axis. Both the tests were carried out with  $k = 1$  and  $\tau = 5$ .

## Details on the systems and their numerical integration

We report below the explicit equations of the coupled dynamical systems and all the useful details on the time series generations and analysis. All the analysis were carried out discarding the first 5000 steps of the generated time series.

### Rössler systems

In the unidirectional case  $X \rightarrow Y$ , the equations of the coupled Rössler systems are

$$\dot{x}_1(t) = -\omega_1 x_2(t) - x_3(t) \quad (23a)$$

$$\dot{x}_2(t) = \omega_1 x_1(t) + 0.15 x_2(t) \quad (23b)$$

$$\dot{x}_3(t) = 0.2 + x_3(t) [x_1(t) - 10] \quad (23c)$$

$$\dot{y}_1(t) = -\omega_2 y_2(t) - y_3(t) + \varepsilon (x_1(t) - y_1(t)) \quad (23d)$$

$$\dot{y}_2(t) = \omega_2 y_1(t) + 0.15 y_2(t) \quad (23e)$$

$$\dot{y}_3(t) = 0.2 + y_3(t) [y_1(t) - 10], \quad (23f)$$

with  $\omega_1 = \omega_2 = 1.1015$  for the case of identical systems, and  $\omega_1 = 1.1015$ ,  $\omega_2 = 0.985$  for the case of different systems, as studied in Refs. [9, 10]. The term  $\varepsilon_{Y \rightarrow X} (y_1(t) - x_1(t))$  was added to Eq. (23a) in the bidirectional tests. Following Ref. [10], the initial state of system  $X$  was set to (11.120979, 17.496796, 51.023544), while the system  $Y$  was initialized by multiplying these values for a random number between 0.5 and 1.5. For all the tested values of the coupling constants, the equations were integrated with a fixed step size of 0.0785 and downsampling the series with a frequency of 1/4, resulting in a sampling step of 0.314 and 105000 total samples.

### Lorenz systems

The bidirectionally coupled Lorenz systems are defined by the following equations:

$$\dot{x}_1(t) = 10(x_2(t) - x_1(t)) \quad (24a)$$

$$\dot{x}_2(t) = x_1(t)(28 - x_3(t)) - x_2(t) + \varepsilon_{21} y_1^2(t) \quad (24b)$$

$$\dot{x}_3(t) = x_1(t)x_2(t) - 8/3 x_3(t) \quad (24c)$$

$$\dot{y}_1(t) = 10(y_2(t) - y_1(t)) \quad (24d)$$

$$\dot{y}_2(t) = y_1(t)(28 - y_3(t)) - y_2(t) + \varepsilon_{12} x_1^2(t) \quad (24e)$$

$$\dot{y}_3(t) = y_1(t)y_2(t) - 8/3 y_3(t) \quad (24f)$$

The equations were integrated using the time step  $dt = 0.01$ , initializing the system  $X$  to (1, 1, 1) and choosing the initial point for  $Y$  with the same random criterion used for the Rössler systems. The resulting time series were saved with a downsampling frequency of 1/5, resulting in a sampling step of 0.05 and 205000 total samples.

## Lorenz 96 systems

Using the conventions  $x_{-1} = x_{N-1}$ ,  $x_0 = x_N$  and  $x_{N+1} = x_1$ , the equations of the 40-dimensional unidirectionally coupled Lorenz 96 systems employed in the tests are

$$\dot{x}_i = (x_{i+1} - x_{i-2})x_{i-1} - x_i + F_X, \quad (25a)$$

$$\dot{y}_i = (y_{i+1} - y_{i-2})y_{i-1} - y_i + F_Y + \varepsilon x_i, \quad (25b)$$

with  $i = 1, \dots, 40$ . The initial states were set to  $x_i(0) = F_X + 0.01$  and  $y_i(0) = F_Y + 0.01$ . The equations were integrated with the time step  $dt = 0.03$  and the trajectories were downsampled with frequency  $1/2$ . The tests reported in Fig. 3 and Fig. 4 were carried out using trajectories with 252500 points, while each value of the Imbalance Gain reported in Fig. 5 was obtained by averaging the results obtained from 20 independent realizations with 752000 points.

## Comparison with Extended GC on the EEG data set

Using the same notation that we employed throughout the main text of the paper, the Extended Granger Causality method [11] tries to assess whether  $x$  has a causal influence on  $y$  by studying which one among the two autoregressive models

$$y(t + \tau_e) = \sum_{j=1}^E \alpha_j y(t + (j-1)\tau_e) + \varepsilon_y \quad (26a)$$

$$y(t + \tau_e) = \sum_{j=1}^E \left[ \beta_j y(t + (j-1)\tau_e) + \gamma_j x(t + (j-1)\tau_e) \right] + \varepsilon_{y|x} \quad (26b)$$

gives the best description of the unknown dynamics, performing several local regressions according to Eqs. (26) instead of a single global fit as in standard GC. Each local regression is carried out by sampling a random point in the space of time-delay embeddings and considering the neighbor points within a radius  $\delta$  from the central one, as measured by the Euclidean distance in the space of the joint embeddings  $(x(t), \dots, x(t - (E-1)\tau_e), y(t), \dots, y(t - (E-1)\tau_e))$ . Equivalently, in this work we defined the neighborhood size by fixing the number of neighbors  $k$ . The residuals estimated in each local regression are used to compute the Extended GC index  $\Delta_{x \rightarrow y} = \langle 1 - \varepsilon_{y|x} / \varepsilon_x \rangle$ , which identifies the presence of a coupling when it is statistically different from zero.

As the method was proposed for time series only, we extended it to the case where  $x$  is a static variable by replacing Eq. (26b) with

$$y(t + \tau_e) = \sum_{j=1}^E \beta_j y(t + (j-1)\tau_e) + \gamma x + \varepsilon_{y|x} \quad (27)$$

and we applied it to the case where  $x$  is the duration of the comparison stimulus in the EEG experiment. Since the single EEG time series do not satisfy the requirement of stationarity, similarly to our approach we constructed a data set for each  $t$  and each participant using the different trials as independent realizations. Differently from our method, where  $\tau$  and  $\tau_e$  are distinct parameters, the Extended GC approach is constructed with  $\tau = \tau_e$ . For this reason, instead of studying the behaviour of the Extended GC index as a function of the separation  $\tau$  between the predictive window and the predicted point, that would have required changing  $\tau_e$  as well, we scanned the time  $t$  of the predicted point, moved together with the predictive window. In the analysis carried out with our approach, by contrast, the predictive window was kept fixed after the stimulus onset / offset. Panels b) and c) of Fig. S2 show the Extended GC index as a function of  $t$  for the link from stimulus duration and the POz channel, both using the same parameters that we employed to compute the Imbalance Gain and optimizing them separately. Trying different combinations of  $E$  and  $k$  we found that the largest difference between the Extended Granger Causality indices in the offset and onset periods, as well as the minimum rates of false positives in the second scenario, were found for  $E = 5$  and setting  $k$  to the total number of points available for each subject (around 420), namely performing a single global regression. Notably, with these parameters the Extended Granger Causality is equivalent to the standard Granger causality test. The false positive rate reported in the main text was computed, equivalently to our approach, by using a t statistics threshold of  $t = 2.552$  to reject the null hypothesis of the Extended Granger Causality index being equal to zero.

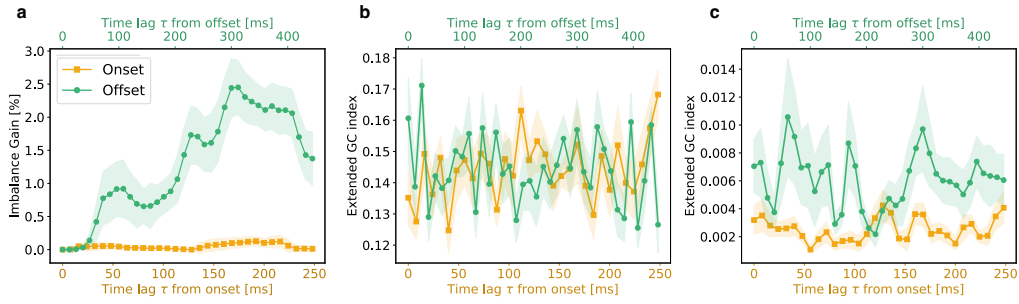


**Figure S2.** Comparison between our method and Extended GC for detecting the link from stimulus duration and the POZ channel, before stimulus onset and stimulus offset. Shaded regions represent the standard error of the mean over the 19 participants. **a)** Imbalance Gain computed with time-delay embeddings of length  $E = 12$  and embedding time  $\tau_e = 12$ , using  $k = 20$ . **b)** Extended GC index as a function of time using similar parameters to the ones employed for the Imbalance Gain in panel a (20 neighborhoods,  $k = 20$ ,  $E = 12$ ,  $\tau_e = 1$ ). Here  $\tau$  represents the first point of the window of length  $E$  used to predict the EEG activity at time  $\tau + E + \tau_e$ . **c)** Extended GC index after optimizing its parameters (1 neighborhood,  $k \sim 420$ ,  $E = 5$ ,  $\tau_e = 1$ ).

## Supplementary images

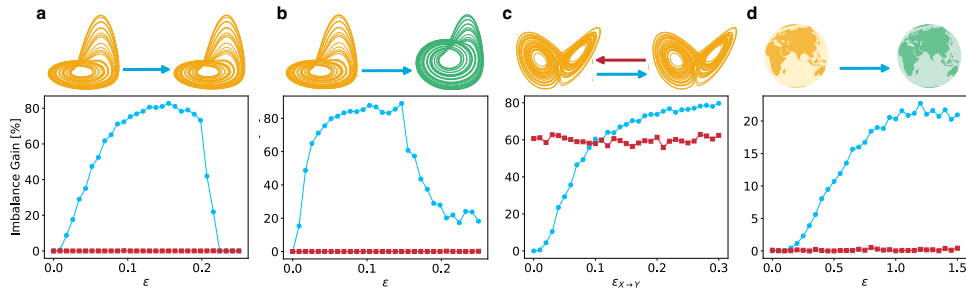


**Figure S3.** Imbalance Gain as a function of the coupling strength for the same pairs of dynamical systems tested in Fig. 3 of the main text, but using all coordinates of the systems instead of time-delay embeddings (3 coordinates for each system in panels **a**, **b** and **c**; 40 variables for each system in panel **d**). The parameters  $\tau$  and  $k$  were set to the same values specified in the caption of Fig. 3.

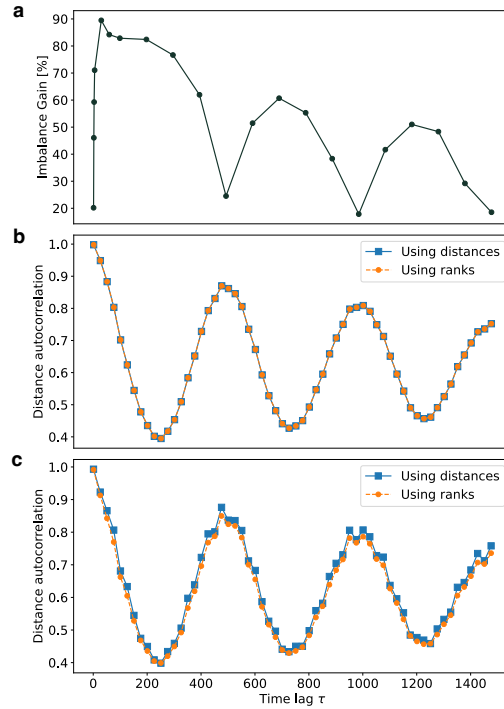


**Figure S4.** **a)**: Imbalance Gain in the  $X \rightarrow Y$  direction for the pair of unidirectionally coupled Rössler systems employed in Fig. 4a of the main text. **b)**: Distance autocorrelation function of the driven system  $Y$ , using the true state space coordinates  $y_1, y_2$  and  $y_3$ . The blue line was computed by means of Euclidean distances as described in Ref. [12], while the orange curve was obtained carrying out the same calculation with ranks, i.e. by replacing the distance matrix  $d_{ij}$  with the rank matrix  $r_{ij}$  before applying the double centering. For this specific system the two curves are almost identical. The local maxima of these curves are related to the minima found by the causality test  $X \rightarrow Y$  in panel **a**, as they correspond to time lags at which the driven system is already maximally predictive with respect to itself. **c)**: As panel **b**, but using time-delay embeddings with  $E = 3$  and  $\tau_e = 5$ .

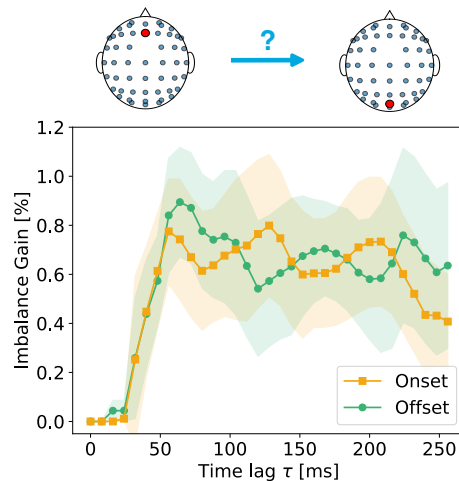


**Figure S5.** Imbalance Gain from the EEG activity of channel Fz to the EEG activity of channel POz, using the same parameters employed in the opposite direction (see Results - EEG experiment).

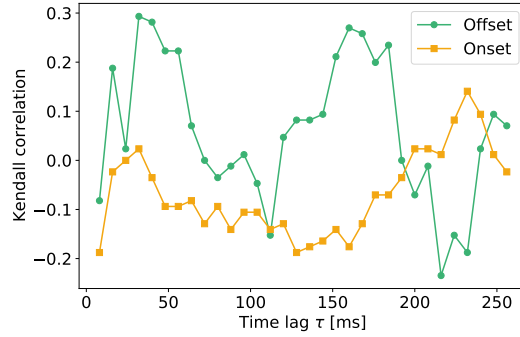


**Figure S6.** Kendall correlation coefficient between the Imbalance Gains of the 19 participants in direction POz  $\rightarrow$  Fz (Fig. 6 of the main text, panel c) and their accuracies in the evaluation of the comparison stimulus' duration, as a function of the time lag  $\tau$  from stimulus onset / offset. The accuracy of each participant is defined as the number of correct answers divided by the total number of trials.

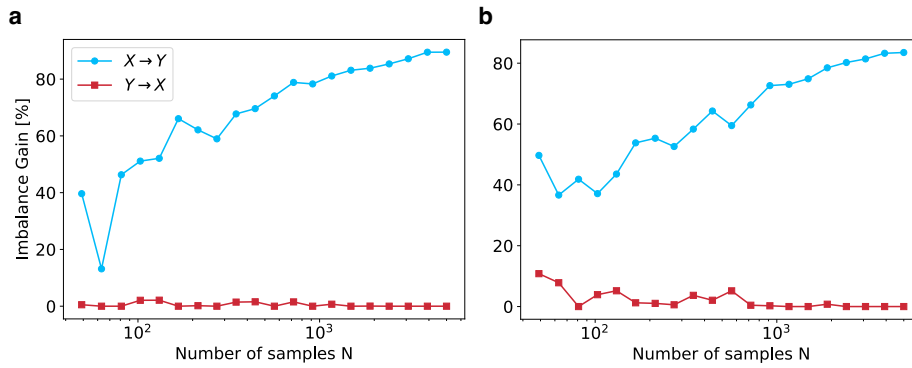


**Figure S7.** Imbalance Gain as a function of the number of samples  $N$ , for different Rössler systems linked in direction  $X \rightarrow Y$  with coupling  $\varepsilon = 0.1035$ , **a)** using all coordinates of each system and **b)** using time-delay embeddings with  $E = 3$  and  $\tau_e = 1$ . In both the cases we set  $k = 1$  and  $\tau = 30$ .

## Supplementary references

- [1] G. Casella and R. Berger. *Statistical Inference*. Duxbury Resource Center, 2001.
- [2] R. B. Nelsen. *An introduction to copulas. The Science of Microfabrication*. Springer, New York, 2006.
- [3] R. S. Calsaverini and R. Vicente. “An information-theoretic approach to statistical dependence: Copula information”. *Europhys. Lett.* **88**, 68003 (2009).
- [4] H. Safaai et al. “Information estimation using nonparametric copulas”. *Phys. Rev. E* **98**, 68003 (2018).
- [5] A. Glielmo et al. “Ranking the information content of distance measures”. *PNAS Nexus* **1** (2022). pgac039.
- [6] D. Chicharro and R. G. Andrzejak. “Reliable detection of directional couplings using rank statistics”. *Phys. Rev. E* **80**, 026217 (2009).
- [7] A. Krakovská and F. Hanzely. “Testing for causality in reconstructed state spaces by an optimized mixed prediction method”. *Phys. Rev. E* **94**, 052203 (2016).
- [8] E. N. Lorenz. “Atmospheric Predictability as Revealed by Naturally Occurring Analogues”. *Journal of Atmospheric Sciences* **26**, 636 - 646 (1969).
- [9] M. Paluš and M. Vejmelka. “Directionality of coupling from bivariate time series: How to avoid false causalities and missed connections”. *Phys. Rev. E* **75**, 056211 (2007).
- [10] M. Paluš et al. “Causality, dynamical systems and the arrow of time”. *Chaos* **28**, 075307 (2018).
- [11] Y. Chen et al. “Analyzing multiple nonlinear time series with extended Granger causality”. *Physics Letters A* **324**, 26-35 (2004).
- [12] C. F. O. Mendes, R. M. da Silva, and M. W. Beims. “Decay of the distance autocorrelation and Lyapunov exponents”. *Phys. Rev. E* **99**, 062206 (2019).